Tunable Piezoelectric Vibration Energy Harvester With Supercapacitors for WSN in an Industrial Environment

Florian Huet, Vincent Boitier, and Lionel Seguier

***Abstract*—This article presents the design strategy and experimental validation of a battery-free power supply for wireless sensor nodes (WSN) on an industrial study case. The power supply is based on the principle of vibration energy harvesting (VEH). The general architecture of the linear generator with electronic is presented. It is composed of commercially available components as a MIDE PPA 1014 piezoelectric cantilever beam and a LTC3588 circuit to extract and shape the electrical energy. The energy source comes from mechanical vibrations measured on the industrial environment in operation. A tunable mechanism of the resonance frequency is added in order to have a wider range of use than the natural range of a linear harvester. To adapt the VEH according with the source, it resonant frequency range can be tuned with a dedicated tip-mass. Then a fine adjustment within a range of about 20 Hz is set using both a moving clamping device and a temporarily wired electronic device working as a maximum power point finder (MPPF). To achieve a long lifetime, the storage is done using balanced supercapacitors. Two operational demonstrators are shown. The test benches as well as numerous experimental tests are presented. Shaped according to the industrial environment (49.0 Hz @ 2.7 m/s^2), the VEH is capable of delivering continuously 100mA@3.3V with 200 mA peaks. When the power harvested ($\approx$ 2.9 mW) is upper than the sensor average power, it offers the capability to store 17.5 J at 18.5 V. As a result, from this work, a WSN can successfully operate over a significantly long period of time despite fluctuations in the vibration source.**

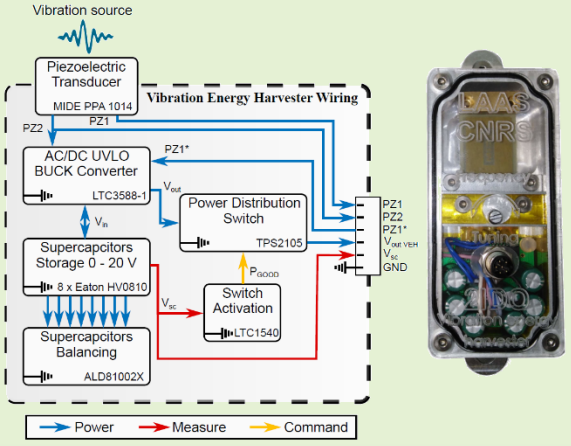

***Index Terms*—Piezoelectric generator, vibration energy harvesting, energy management, tuning frequency, supercapacitor.**

I. Introduction

THE deployment of IoT (Internet of Things) in the industrial, transport, and health sectors is soaring over the past few year. The control of the measurement at each step of a system becomes a necessity to aim the objectives of performance improvement. The integration of wireless sensor nodes (WSN) is one of the considered solutions. However, few systems are currently deployed so far. Companies like Libelium [1] offer a vision of a smart city, in which their sensors can be deployed to collect several environmental data. WSN can be used in public infrastructure for monitoring, such as the Los Angeles Golden Gate [2], where vibration sensors monitor the integrity of the structure over time. Researchers are using WSNs to understand the behavior of seabirds nesting on Great Duck Island by collecting physical data from the site (temperature, moisture, or pressure) [3]. Still, the monitoring of the Tungurahua volcano is made with WSN carrying seismographs [4]. However, the energy autonomy of the latter hinders their deployment [5], [6]. While the number of connected devices is increasing, it is then imperative to find alternative solutions for battery sources to prevent the global energy consumption following the same trend.

Many solutions exploit ambient energy sources to power WSN [7]. The nature of the harvested energy depends on the environment close to the node sensor. It is possible to recover thermal, solar, vibratory energy, and many others

Manuscript received 8 April 2022; revised 9 June 2022; accepted 18 June 2022. Date of publication 28 June 2022; date of current version 1 August 2022. This work was supported in part by the Internet Industriel des Objets et des Opérateurs (2IDO) Project through the Banque Publique d'Investissement (BPI) and in part by the Programme d'Investissements d'Avenir (PIA). The associate editor coordinating the review of this article and approving it for publication was Dr. Ali Mohammadi. *(Corresponding author: Florian Huet.)*

Florian Huet is with the LISPEN, Arts et Metiers Institute of Technology, HESAM Université, 13617 Aix-en-Provence, France (e-mail: florian.huet@ensam.eu).

Vincent Boitier and Lionel Seguier are with the LAAS, Université de Toulouse, 31400 Toulouse, France (vboitier@laas.fr; lseguier@laas.fr).

Digital Object Identifier 10.1109/JSEN.2022.3185426

[8]. In this case, we are interested in the exploitation of vibration energy that is present in industrial installations. Compared to other sources, this one does not have [9]–[14] the best energy potential. However, it has the advantage to be consistently available on industrial sites. Vibration sources are not very sensitive to meteorological conditions compared to sun radiations or natural air flow variations.

In the field of vibration energy harvesting (VEH), industrial companies [15]–[18], have created some systems but very few remain to this day. The architectures commonly used are based on the principle of a linear inertial resonator. The employment of this system guarantees a simplicity of implementation and operation, which results in an efficient operation. However, this efficiency can be drastically reduced due to the thinness of the bandwidth. To ensure the electromechanical conversion, an electroactive element is coupled to the structure. In order converts the mechanical energy that is transmitted to a seismic mass into electrical energy. Electromagnetism, magnetostriction, electrostatic, or piezoelectric effects can be employed. In literature, many laboratories develop different systems to expand the covered range of use. These solutions propose to widen the operating bandwidth by introducing non-linear systems with hardening/softening stiffness [19]–[21], bi-stable systems [22]–[24], active systems [25]–[27], and other systems [28]–[30]. These solutions are for the moment difficult to be implemented with the elements that are commercially available. The use of piezoelectric generators for energy harvesting is well studied and simple to be implemented [31]. This article, presents the implementation of a solution based on linear piezoelectric generator and adaptable.

The classical structure used in linear HEV is the cantilever beam. It is envisaged to stress this structure at resonance in order to extract maximum energy. An adjustment of this frequency is then necessary. Two simple methods can be considered: the modification of the frequency or the modification of the seismic force applied by the mass. For the first approach the clamp can be mobile. The work of Wang *et al.* [32] shows a system of sliding clamp allowing to vary the frequency by more or less 69 % compared to the resonance frequency of 580 Hz. This solution produces up to 22 μW for an acceleration of 1 m/s^2. The work of Huang *et al.* [33] presents a rolling clamp solution. The frequency is 121 Hz with a possible variation of 80%. The power is estimated at 84 μW but the acceleration is not expressed. In the second approach we find devices with moving masses which modify the center of application of the seismic force. Schaufuss *et al.* [34] proposes to slide the mass with a screw. The resonance frequency is 42 Hz with a variation of 31 %. It produces 80 μW for an acceleration of 0.3 m/s^2. The work of Chandwani *et al.* [35], [36] shows a solution of automatic adjustment with cylindrical masses moving at the end of the beam. This solution can provide 13.18 μW at a frequency of 21 Hz and an acceleration of 10.4 m/s^2. The operating range is 66 %.

In general, tunable linear VEHs can produce power in the range of a few microwatts to a few milliwatts [32]–[36] in volumes considered acceptable by the industrial community (25 mm × 50 mm × 70 mm) to promote their integration into systems. Such level of power is not able to directly supply a sensor, either by its amplitude or by its shape. It is necessary to store the energy during the period of low consumption of WSN and to draw it from the storage during the high energy-consuming period. It is also essential for this scenario to take into account the variability or the stops of the vibratory source. The energy can be stored on batteries but also in supercapacitors. A better resilience over time of the electrochemical solution is usually achieved. In addition, supercapacitors accept more cycles and are less sensitive to temperature than batteries. Some commercial circuits are dedicated to VEH. They perform all three necessary steps for VEH: energy extraction, shaping and management of the stored energy. However, the efficiency is moderate (<40 %) due to impedance matching problems. For piezoelectric devices, the commercial LTC3588-1 circuit [37] is commonly used, but its architecture is rarely optimized [38]–[41]. Although some high-efficiency non-linear extraction circuits are also developed in the academic world (SSHI, SSHS, SECE ...) [8], [42]–[44], these systems are not available in the market yet.

In this article, a novel strategy for the development of tunable piezoelectric VEHs for WSNs is proposed. The vibration sources come from industrial environments identified and measured with equipment developed in this work. The paper shows the design and implementation phases of demonstrators. Each VEH is composed of a piezoelectric energy conversion element, an extraction circuit, and a storage block based on supercapacitors. All components used in the proposed system are commercially available. The on-site tuning system offers versatility in the use of the harvesters. Through a maximum power display device, the VEHs can be easily adapted to the vibration source for optimal energy extraction. Many experimental validations are presented to validate the insights. The impact of mechanical charging, the frequency tuning with a simulated vibration source and a WSN power in real-condition test is also highlighted.

II. Global Architecture and Environment

A. Piezoelectric Generator Architectures

This work presents a device for the vibration energy harvesting with adjustable resonance frequency. A well-know structure of piezoelectric beam cantilever is used to achieve the energy generation. It is also composed of a complete electronic system for the management of the extracted energy, in order to supply WSN. The overall architecture of the complete VEH system adapted to power WSN is shown in Fig. 1.

Piezoelectric transduction is employed to convert vibrational energy into electrical energy. For this purpose, a resonant system is used, consisting of a MIDE PPA 1014 piezoelectric beam clamped on one side and free at the other (cantilever beam). On the free side, a seismic mass must be chosen to coarsely target the frequency range. By adjusting the position of the clamping (length of the beam) it is possible to adjust accurately the resonance frequency at the vibration source. This maximizes the deformations within the piezoelectric patch and optimizes the mechanical coupling with the source resulting to an optimized energy conversion. The signal produced by the transducer is not directly usable: its high voltage, very low current, and the alternative form must be shaped to be used by WSN. For that, an extraction circuit is adapted

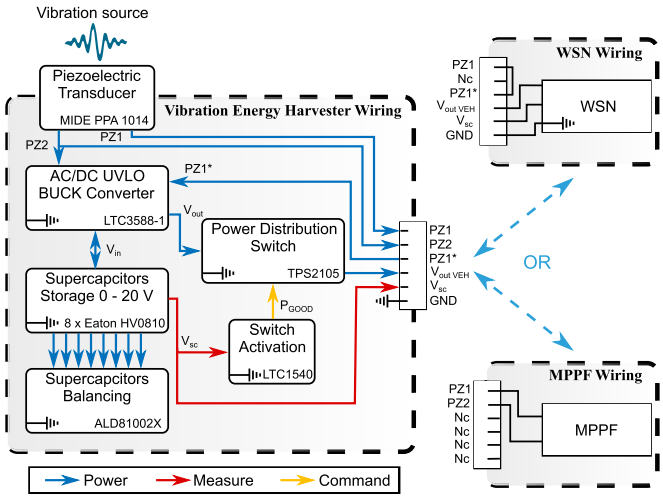

Fig. 1. Block diagram architecture of the VEH device.

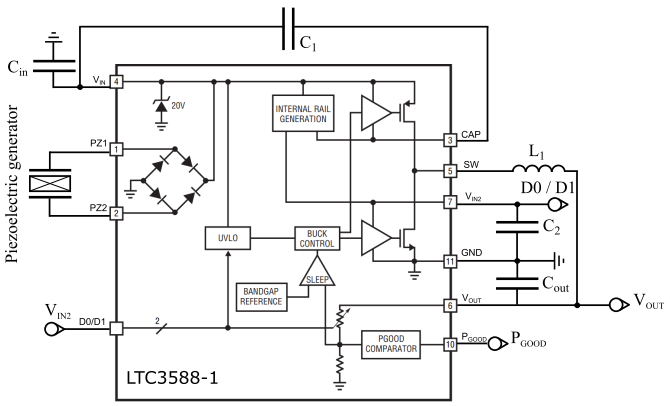

Fig. 2. Extraction circuit with environment block diagram.

for the harvesting of vibratory energy (LTC3588-1 (Fig. 2)). This circuit allows to rectify a signal up to 20.0 V (hereafter the signal is clipped by an internal Zener diode), to smooth, to store and reduce the output voltage to 3.3 V (adjustable voltage level) with a maximum current of 100.0 mA. The activation of the output voltage requires a minimum rectified input voltage level of 5.1 V, and the deactivation is performed when the input voltage level is below 3.7 V.

The LTC 3588-1 circuit collects the electrical energy. A storage block composed of eight supercapacitors (Eaton HV0810) in series allows the storage of the energy to perform the start-up phase of WSN and to store the overproduction thereafter. A balancing system (ALD810023) is added to ensure that the supercapacitors are used correctly. Too much imbalance would reduce the life of these components. A hysteresis comparator (LTC1540 [45]) is placed to activate or deactivate the output voltage by closing or opening a power distribution switch (TPS2105) when a predefined storage voltage is reached.

The transducer and electronics are encapsulated in a specially designed waterproof housing, which forms a regulated power source. This box allows the adjustment of the piezoelectric beam length to set the resonant frequency of the transducer at the vibration frequency of the source. A connector is used to connect two systems on the VEH. The first one is a maximum power point finder (MPPF), which is a device dedicated to tune the VEH resonance frequency to the vibration frequency of the source. The second one is WSN. Without any element connected to the VEH, the piezoelectric element is disconnected from the electronics and the circuit is not solicited. When the MPPF is connected to the VEH, this device measures and displays the voltage at the terminal of the piezoelectric element. It allows accurate tuning as the voltage is maximum when the resonant frequency is synchronized with the excitation. When WSN is connected, it closes the circuit of the piezoelectric element and allows the proper functioning of the electronics. The selection, dimensioning, and characterization of all the technological components are detailed in the following sections and in a previous work [46].

B. Industrial Environment Vibrations

To have an assessment of the energy potential, numerous measurements were performed on various industrial equipment. The measurements were executed with a system developed in the laboratory, Fig. 3. It is composed of a NI-USB 6008 acquisition card, a 3-axis accelerometer ADXL354 with a bandwidth of 2 kHz and a computer with Labwindows® software. The sensor is encapsulated in a prototyped housing (FDM) equipped with NdFeB magnets for quick positioning on magnetic surfaces. The measurements were carried out on motor pump units and vacuum pumps that are used for the operation of the LAAS-CNRS white room (Fig. 3), as well as on a gas burner (Fig. 4) of a TOTAL refinery.

On the pump, four measurements in different areas were done. The pump consists of a single-phase synchronous motor and a two-stage lubricated rotary vane pump. In the case of the burner, the whole system is composed of an electric motor, a coupling bearing, a fan (blower), a second coupling bearing, a reduction gear, and a turbine. Seven interesting measuring points have been identified on the structure. The main objective was to be able to instrument such structures with a WSN and to retrieve simple information such as the temperature of the motor pumps. More complex information can be retrieved, such as vibrations in the case of preventive maintenance of the burner.

The Fig. 5 represents the FFT from the time signal measured during the test represented in Fig. 3. It highlights the complexity of the source vibration signal, which exhibits, multitude of visible peaks. The Y signal correspond to the source of vibration used in section IV.C.

Table I is an extract of the different measurements executed. It lists the frequencies at which the accelerations amplitudes reached a maximum for each axis of the sensor, respectively. One can identify on LAAS-CNRS equipment a fundamental in the three directions at a frequency of 49.0 Hz for a maximum acceleration of 2.7 m/s^2 in the Y-axis (transverse to the axis of rotation of the pump shaft). Concerning the TOTAL machine, one can identify an interesting source at the frequency of 100 Hz for a maximum acceleration of 2.2 m/s^2 on the Z-axis (axis of rotation of the motor).

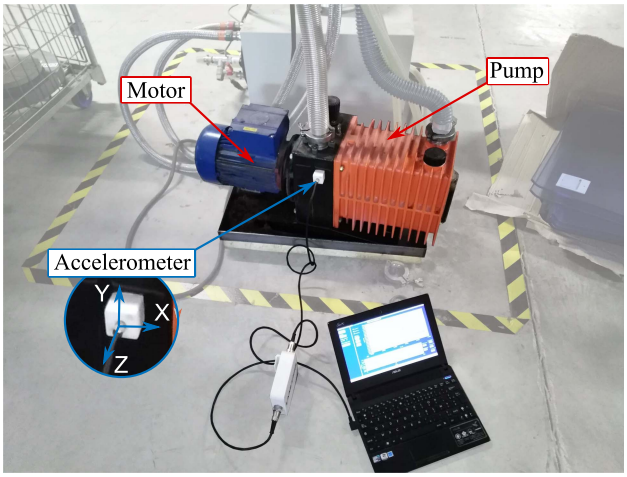

Fig. 3. Vacuum pump vibration measurements.

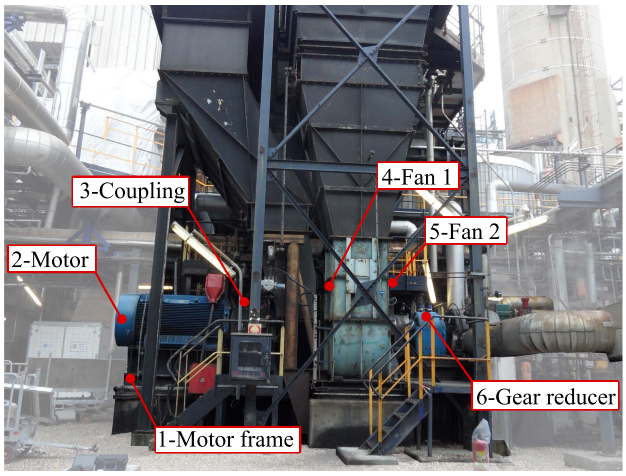

Fig. 4. TOTAL gas burner.

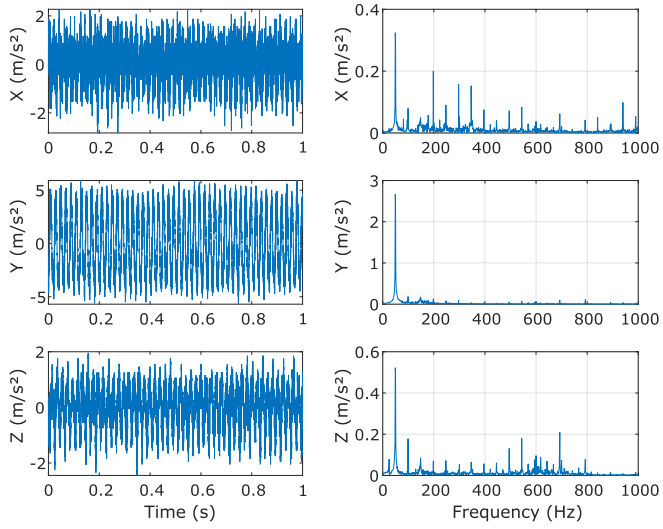

Fig. 5. Temporal and fast fourier transform of triaxial accelerations signals from the vacuum pump.

Based on these measurements, it is possible to identify the potential of the presented sources and to dimension an energy recovery unit according to the characteristics of the vibration source. We can notice that there are vibrations available to harvest the energy, but their frequency or amplitude are not predictable and can be different according to the axis of solicitation. This is a common drawback for this type of system. The solution provided in this article allows adjusting the resonant frequency of the resonator according to the source. However, the acceptable range of variation is a few tens of Hertz. We then choose sources with the highest possible acceleration and at low frequencies (<100 Hz). A measurement phase on site is systematically necessary in order to identify the region of the machine where to install the VEH and to define its pre-setting.

TABLE I
EXTRACT OF THE MEASUREMENTS CARRIED OUT ON INDUSTRIAL EQUIPMENT

Meas.	X		Y		Z	
	Freq. (Hz)	Amp. (m/s²)	Freq. (Hz)	Amp. (m/s²)	Freq. (Hz)	Amp. (m/s²)
Pump	49.0	0.3	49.0	2.7	49.0	0.5
Burner	50.0	0.6	236.0	0.5	100.0	2.2

III. PIEZOELECTRIC HARVESTER DEVELOPMENT

A. Electromechanical Conversion Design

The electromechanical conversion system is based on the conventional structure [40] of a commercially available piezoelectric cantilever beam (MIDE PPA 1014 [47]) with a seismic mass placed at its end. With a movable clamp, the resonant frequency of the system can be set (more detail in section III.B). Table II lists the different characteristics and dimensions of the beam. MIDE's piezoelectric beams are composed of a stack of different layers (FR4, copper electrode, PZT, copper, and FR4). The two layers of FR4 are of different thicknesses to offset the piezoelectric patch from the neutral line of the beam and thus obtain a unimorph beam. Thus and thus, the PZT is only stressed in tension or compression when the beam is bent. Copper sheets are used to harvest the charges produced.

The seismic mass employed allows setting the operating frequency range. The beam has been characterized with different masses; this is detailed in the experimental part. The characterization allows identifying some model parameters such as damping. This type of generator can be modelled as a mass-spring-damper system with one degree of freedom and a linear coupling coefficient. Equations (1) and (2) present the dynamically coupled mechanical and electrical behavior respectively.

$$\ddot{x} + \frac{\omega_0}{Q}\dot{x} + \omega_0^2 x + \frac{\alpha}{m}V = \gamma \tag{1}$$

$$\alpha\dot{x} - C_0\dot{V} = \frac{V}{r_l} \tag{2}$$

$$\omega_0 = \sqrt{\frac{k}{m}} \tag{3}$$

In these relations (Equations (1) and (2)), ω_0 represents the eigen pulse; Q is the quality factor, which is related to the damping; α is the electromechanical coupling coefficient; γ is the external excitation; x, $\dot{x}$ and $\ddot{x}$ correspond respectively to the displacement, velocity, and acceleration of the seismic

TABLE II
MIDE PPA 1014 CHARACTERISTICS

Parameters	Value (mm)	Parameters	Value (mm)
Total length	53	Total width b	20.8
Piezoelectric length	27.8	Piezoelectric width	18
Total thickness h	0.71		

MULTI LAYER STRUCTURE

Layer material	Thickness (µm)
FR4	80
Copper	30
PZT 5H	190
Copper	30
FR4	360
Total	710

ELECTROMECHANICAL PARAMETERS

Electromechanical parameter	Value at Clamp 0
Capacitance (nF)	40
Global mass (g)	2
Effective mass m_0 (g)	0.339
Stiffness k (N/m)	2187.85
Max deflection (mm)	2.5
Max voltage range (V)	150

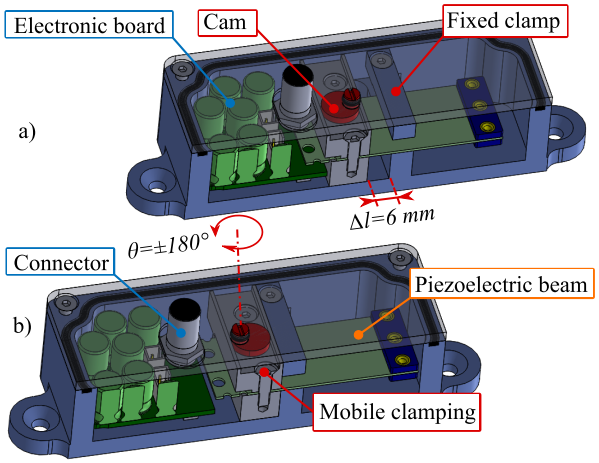

Fig. 6. Tuning frequency system representation, (a) high and (b) low frequency position (sectional view).

mass concerning the frame. In the electrical relation, we find the electromechanical coupling coefficient and the electrical capacitance C_0 of the piezoelectric element and a load resistance r_l connected to the terminals of the piezoelectric element. V and $\dot{V}$ are the voltage across the resistor and its time derivative. Equation (3) represents the relationship between the pulsation ω_0, the beam stiffness k and the dynamic mass m. The modification of these two parameters influence the mechanical behavior of the structure. We can take advantage of this to adjust the resonance frequency ($f_0 = \omega_0/2\pi$) of the VEH.

B. Tuning Frequency System

One of the major problems of an energy harvesting device is the correspondence between the resonant frequency of the harvester and the source of vibration. Ideally, it is necessary to use broadband devices capable of providing at least half of their maximum power over a wide frequency spectrum (>10 Hz). The use of a highly damped or non-linear system makes it possible to obtain a wide spectrum. In the first case, the maximum power can be drastically reduced. In the second case, the systems are more complex and, to our knowledge, there is no device on the market capable of meeting this demand. However, laboratory solutions under development may be able to solve this issue [19]–[30]. During this project, a linear system have been deployed whose resonance frequency can be adjusted to match with the source on-site. For this purpose, a device for adjusting the clamping length has been integrated. To adjust the resonant frequency, it is possible to modify the tip mass or the length. First, a mass for coarse adjustment is selected. Then the clamping length, which is accessible from outside, is set for a fine adjustment of the resonant frequency. The demonstrators presented in section III.D have the following characteristics:

- Tip mass 26.8 g; f_{min}48.0 Hz; f_{max} 66.0 Hz
- Tip mass 13.0 g; f_{min} 69.0 Hz; f_{max} 94.4 Hz

Fig. 6 shows the composition of the mechanical system. It is composed of two sub-assemblies: the housing (fixed part) and the active element (moving part). The first one allows the encapsulation of the VEH and the electronics, but it also has a sliding link (fixed clamping) where the piezoelectric beam can slide. The second one is composed of a beam that has a seismic mass on one side, and a mobile clamping on the other side. The mobile clamping can slide freely inside the case. By turning the cam (the red part), the mobile clamping can be moved forwards and backwards. When the cam is at the 0 ° position, the clamping length is 27 mm. When the cam is at the 180 ° position, the length is 21 mm (total variation of 6 mm).

The action on the cam has the effect of modifying the length (L) of the beam. This action has the consequence of changing the stiffness k (Equation (4)) and the seismic mass m (Equation (5)) of the system. As result, the resonance frequency f_0 (Equation (3)) is then adjustable.

$$k = \frac{3EI}{L^3} \quad \text{with } I = \frac{bh^3}{12} \tag{4}$$

$$m = \frac{\Delta m}{\Delta L}(L - L_0) + m_{tip\_mass} + m_0 \tag{5}$$

Equations (3) and (4) and the geometrical data available in the MIDE PPA 1014 beam technical document (Table II) define all the modelling parameters: width b; thickness h; stiffness k as a function of length L for a beam in no-load condition ($m = m_0$). With geometrical parameters, it is possible to identify the quadratic moment (I) of 0.6 mm^4 and an equivalent modulus of elasticity (E) of 24.7 GPa with material parameters. By adding mass (m_{tip_mass}) at the end of the beam, the stiffness does not change, contrary to the mass (Equation (5)).

The latter has a linear behavior that depends on:

- the variation of the mass ($\Delta m = 0.1$ g)
- length variation ($\Delta L = 6$ mm)
- the minimum length of the beam ($L_0 = 21$ mm)
- the minimum empty mass ($m_0 = 0.2$ g)

Fig. 7a shows, as a function of length, the evolution of stiffness in blue and mass in red. Fig. 7b represents the evolution of the frequency for two particular values of m_{tip_mass} ($m_1 = 13.0$ g and $m_2 = 26.8$ g). The cross and circle marks represent the experimental values of the final demonstrators presented in the following sections. It can be noted a very good

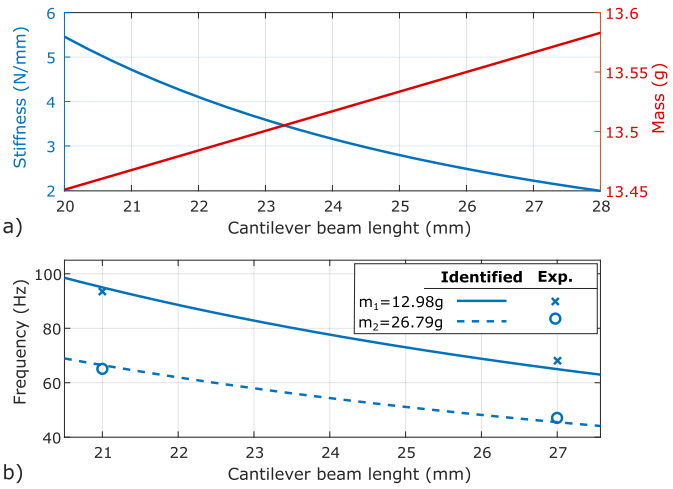

Fig. 7. k, m (a) and f_0 (b) evolution vs beam length (L).

correspondence between the data. For the first loading case (m_{tip_mass} = 13 g), the resonant frequency is from 97.4 Hz to 66.7 Hz, so 30.7 Hz of total adjustment range. For the second loading case (m_{tip_mass} = 26.8 g), the frequency is from 68.2 Hz to 46.7 Hz, which gives a total adjustment range of 21.4 Hz.

C. Maximum Power Point Finder

The converted energy is optimal when the resonance frequency of the piezoelectric beam is in agreement with the source excitation frequency. The energy conversion system can identify the optimum operating point based on the supercapacitors voltage. However, since the storage capacity is very high (125.0 mF) compared to the charge current, it becomes difficult to see a voltage variation in real-time. The encapsulation does not allow a mechanical visualization of the beam resonance. Therefore, a maximum power point finder (MPPF) module located at the terminals of the piezoelectric element (Fig. 8) has been developed for this purpose.

The MPPF module is composed of an Arduino Nano that is powered by a 9.0 V battery. The voltage measurement of the piezoelectric beam is rectified and it is smoothed by a capacitor. As the voltage can reach levels too high for the analog input of the Arduino, a protective Zener diode allows obtaining a maximum voltage between 18.0 V and 20.0 V. This voltage level is reduced by a tension divider bridge to obtain a maximum voltage at the Arduino's ADC input of 5.0 V.

The schematic (Fig. 9) shows the composition of the MPPF module. This module is connected via a 6-way connector (Fig. 1). A display screen connected to I2C bus allows the visualization of the voltage level and its evolution by a plot over time, as well as the display of the numerical value in volts. Once the harvester is positioned on a vibration source and it is connected with the MPPF module, the instantaneous voltage produced by the beam is displayed. When adjusting the resonance frequency of the VEH (action on the adjustment screw Fig. 6), it can be observed the voltage evolution as a function of the angle of the screw. As the voltage reaches its maximum, the setting is complete. The connection of the sensor to the generator closes the circuit and allows the storage stage to be charged.

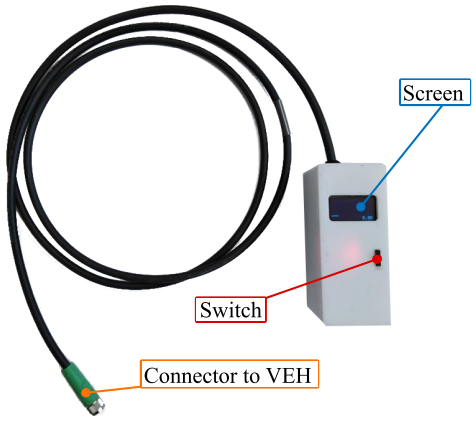

Fig. 8. Maximum power point finder (MPPF).

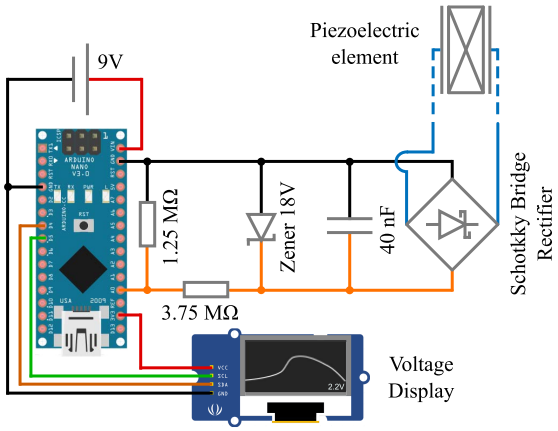

Fig. 9. MPPF module, schematic.

D. Prototyping

Two prototypes have been built to experimentally validate the insights of this article. Only the tip mass (26.8 g and 13.0 g) and the activation voltage threshold are different between both prototypes (7.0 V and 5.1 V). The beam and the length variation induced by the cam are the same. The different characteristics are listed in Table III. The tip mass allows to obtain two different frequency ranges corresponding to the use case seen before (the vacuum pump and the burner). In the case of the first prototype, the triggering threshold is 7.0 V and it allows the execution of four successive starting phases. For the second, the stored energy only covers one starting phase.

The Fig. 10 presents the prototype N°2. An aluminum body has been sized to transmit the vibrations from the source to the seismic mass as much as possible. This housing must be easily integrated into an industrial structure, it measures 9.7 cm × 4.5 cm × 2.7 cm. The surface connector allows connecting the MPPF (Fig. 8) or WSN to be powered (Fig. 16).

The circuits have been designed and built for the devices to integrate all the functionalities (energy extraction and shaping;

TABLE III
PROTOTYPES CHARACTERISTICS

Attribute	Prototype N°1	Prototype N°2
Tip mass	26.8 g	13.0 g
Max. Stiffness	4645.0 N/m	
Min Stiffness	2500.0 N/m	
Max. Freq.	66.0 Hz	94.4 Hz
Min. Freq.	48.0 Hz	69.0 Hz
Activation Voltage	7.0 V	5.1 V
Total weight	255.0 g	241.2 g

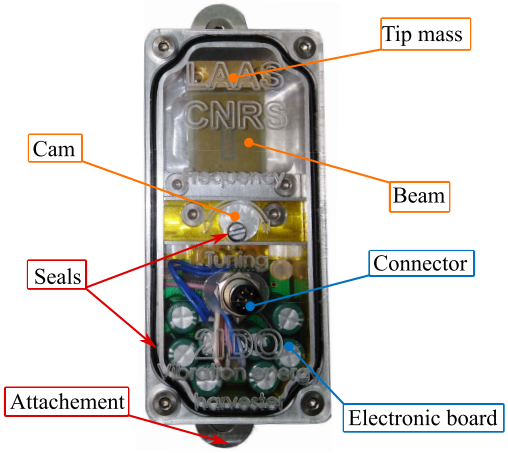

Fig. 10. Prototypes N°2.

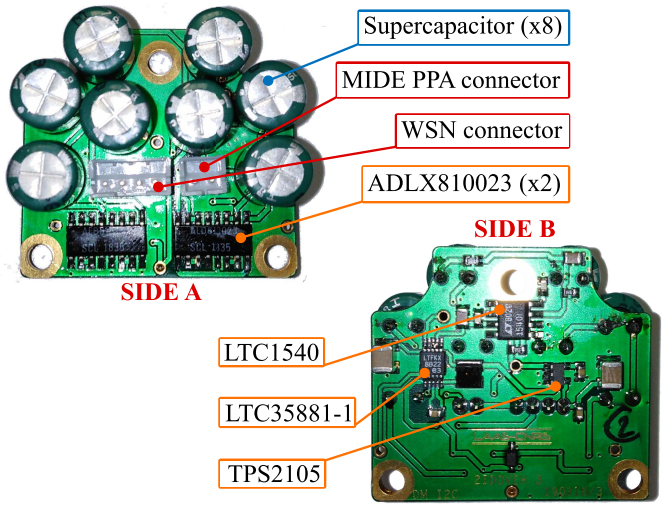

Fig. 11. Electronic board.

storage; supercapacitor balancing; output activation) presented in previously work [40]. Fig. 11 presents these different elements. On one side of the electronic board (side A) is the storage space with eight supercapacitors and the balancing circuits (ALD810023). Connectors are also present to facilitate the connection with the piezoelectric beam and the surface connector. On the other side of the electronic board (side B), we find the extraction circuit (LTC3588-1), as well as the output activation system with the comparator (LTC1540) and the load switch (TPS2105). There are also different passive components (resistors, capacitors, and coil) for the adjustment of the different active components.

E. Sealing and Fixing

The housing has sealing gaskets, a seal between the cover and the frame and two O-rings: one is under the connector; the second one is around the cam axle. The screw recess on the axle is accessible from the outside to adjust the device Two "lobes" extending from the housing are used to attach the harvester to its source of vibration. Two alternatives are available for fixing the housing on the vibration source: using screws or using magnetic attachment. Fig. 10 shows the arrangement of the seal and the high-power (50 N each) holding magnets.

IV. EXPERIMENTAL VALIDATIONS

A. Test Bench

To validate the design of the different elements of the demonstrator, it was necessary to use several characterization systems. First, with an acceleration-controlled test bench to subject the piezoelectric beams to different vibration conditions. This bench allows the characterization of a VEH by sweeping both frequency and load resistance. With this type of experimentation, the optimum operating points can be identified. For this, the following elements are used:

- DSO-X 3014A oscilloscope with function generator
- programmable resistance box MEATEST M642
- Brüel & Kjaer LDS V201 shaker
- Power amplifier
- PCB PIEZOTRONICS 333B32 accelerometer
- Accelerometer signal conditioner
- Computer with Matlab®, Instrument control toolbox, and the Matlab/Agilent driver

These different elements are represented in Fig. 12, and the associated wiring in Fig. 13.

The computer drives the various programmable devices and retrieves the data measured by the oscilloscope. The link is provided by an USB connection and the programming is performed using SCPI language (Standard Commands for Programmable Instruments). The oscilloscope has both the role of a driving card with it integrated function generator and of a measurement card. The function generator allows controlling the frequency and the acceleration level of the excitation of the shaker by adjusting the frequency and the amplitude of the output voltage signal. The power amplifier used to set the shaker in motion amplifies this signal. The accelerometer located on the frame of the generator provides a measurement of the acceleration through the conditioner connected to channel 1 of the oscilloscope. This provides a closed-loop control that is necessary to maintain the test conditions. The piezoelectric generator is connected to the selected load resistor in the programmable resistor box. The voltage measurement at the resistor terminals is done using the channel 2 of the oscilloscope. With this characterization system, one can execute several measurements in reasonable time (compared to manual measurements) while ensuring good accuracy and reliability of the measurements. However, the low loading capacity of the small shaker limits the mass of the tested device or reduces the test conditions (acceleration, frequency).

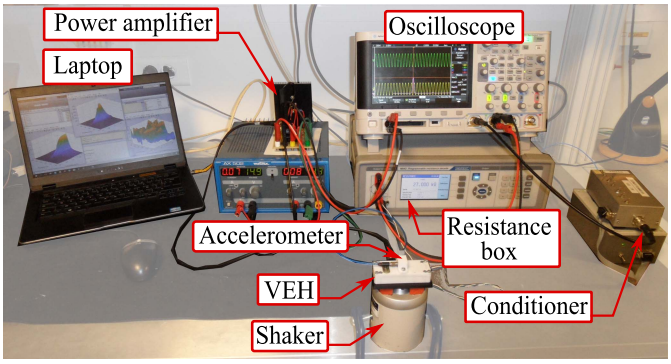

Fig. 12. Constant acceleration test bench.

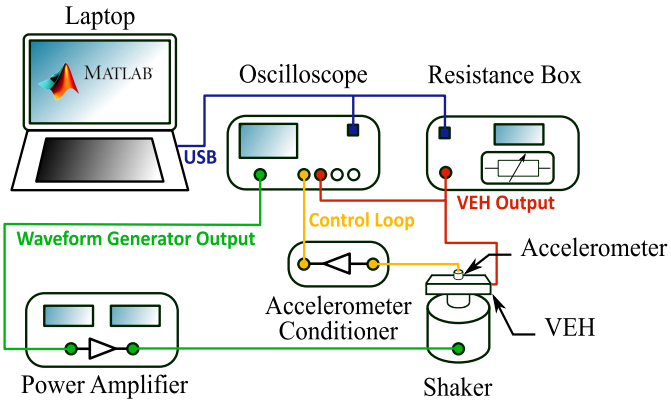

Fig. 13. Test bench connection diagram.

B. VEH Characterization and Frequency Tuning Validation

Tests were carried out using the acceleration-controlled test bench (Fig. 12). The acceleration was limited at 5 m/s^2 for reasons of too high on-board mass for the shaker. The latter being small, the nominal force it provides to the demonstrator remains low. To limit the noise on the excitation by increasing the power of the input signal or by decreasing the acceleration, it is advisable to have a mass in motion as low as possible. The aluminum structure cannot be modified, the tested system corresponds to the whole prototype without electronics, so that the weight of the structure is reduced, and the beam can be characterized only as a function of mass and stiffness. The purpose of the tests is to extract the performance and to model the parameters of the piezoelectric beam. The measurements were carried out for three different masses: 2.0 g, 3.9 g, and 5.9 g. These masses are lower than those of the final demonstrators for the reasons seen previously. The resonance frequency is therefore normally increased compared to the final demonstrators. They also have the role of validating the frequency adjustment system. For each mass, six clamping positions were tested to vary the length between 21 mm and 27 mm, which corresponds to θ being equal to 180 ° and 0 ° respectively. The beam is the longest at the first position. For each of the positions, a frequency sweep (140 Hz to 240 Hz for 2.0 g; 80 Hz to 160 Hz for 3.9 Hz; 80 Hz to 140 Hz for 5.9 g), as well as a load resistance sweep from 1 kΩ to 100 kΩ are performed with a discretization of 25 points for a total of 625 measurements. Fig. 14 shows the example of the VEH

TABLE IV
MAIN CHARACTERISTICS ACCORDING TO THE POSITION OF THE CAM (TIP MASS OF 2.0 g)

Position	f_{res} (Hz)	R_{opt} (kΩ)	V_{opti} (V)	C_0 (nF)	Q	BW (Hz)	P_{max} (μW)
1	156.6	21.5	2.2	47.0	23.4	6.7	218.0
2	163.8	21.5	2.6	45.0	24.1	6.8	303.0
3	167.6	21.5	2.5	44.0	24.6	6.8	300.0
4	171.4	21.5	2.1	43.0	26.7	6.4	191.0
5	179.2	21.5	1.5	41.0	21.3	8.4	104.0
6	200.5	17.7	2.4	44.0	34.0	5.9	327.0

TABLE V
MAIN CHARACTERISTICS ACCORDING TO THE POSITION OF THE CAM (TIP MASS OF 3.9 g)

Position	f_{res} (Hz)	R_{opt} (kΩ)	V_{opti} (V)	C_0 (nF)	Q	BW (Hz)	P_{max} (μW)
1	100.8	31.0	3.2	49.0	26.9	3.7	314.0
2	103.7	31.0	3.1	48.0	27.3	3.7	284.0
3	106.8	26.0	2.8	57.0	29.3	3.6	297.0
4	113.1	26.0	2.1	53.0	23.6	4.6	155.0
5	116.4	26.0	1.6	52.0	24.3	4.9	92.0
6	123.1	26.0	1.4	51.0	15.4	9.2	15.0

TABLE VI
MAIN CHARACTERISTICS ACCORDING TO THE POSITION OF THE CAM (TIP MASS OF 5.9 g)

Position	f_{res} (Hz)	R_{opt} (kΩ)	V_{opti} (V)	C_0 (nF)	Q	BW (Hz)	P_{max} (μW)
1	87.8	31.0	7.7	57.0	30.9	2.8	1887.0
2	92.1	31.0	7.8	55.0	32.1	2.8	1967.0
3	96.4	31.0	7.4	52.0	32.7	2.9	1737.0
4	101.1	38.0	7.1	41.0	31.1	3.3	1282.0
5	105.8	38.0	5.8	39.0	30.1	3.5	885.0
6	110.9	26.0	3.1	55.0	30.7	3.6	377.0

with a 5.9 g tip mass. The voltage across the load resistance and generator power is observed as a function of resistance and excitation frequency. A power peak corresponding to the optimum operating point can be observed. This point depends on the clamping length. From this point, different performance criteria and modelling parameters can be identified: resonance frequency (f_{res}), maximum power (P_{max}), optimal load resistance (R_{opti}), optimal voltage (V_{opti}), beam capacitor (C_0), quality factor (Q), and bandwidth (BW).

Tables IV, V and VI contain the items identified for each load case (mass and clamping length). On average over all the tests, the mean electrical capacity of 48.5 nF was found, which is coherent with the 40.0 nF described in the technical documentation. Overall, the bandwidth is very small and it ranges from 2.8 Hz to 9.2 Hz, which was expected for a linear generator. The quality factor is between 15.4 and 34.0 and at an average value of 27.1, which allows a good power availability despite frequency variations. Since all VEHs were tested in a similar frequency range, the optimum load resistance found is between 17.7 kΩ and 38.0 kΩ.

The results on Table IV and V show a voltage at the optimum operating point below 5.1 V (the voltage at which the energy stored is transferred out of the circuit). In these two cases, it will not be possible to supply the sensor. With regard to the consumption of the sensor (Table VII), the power supplied by the generator is, in most of the cases,

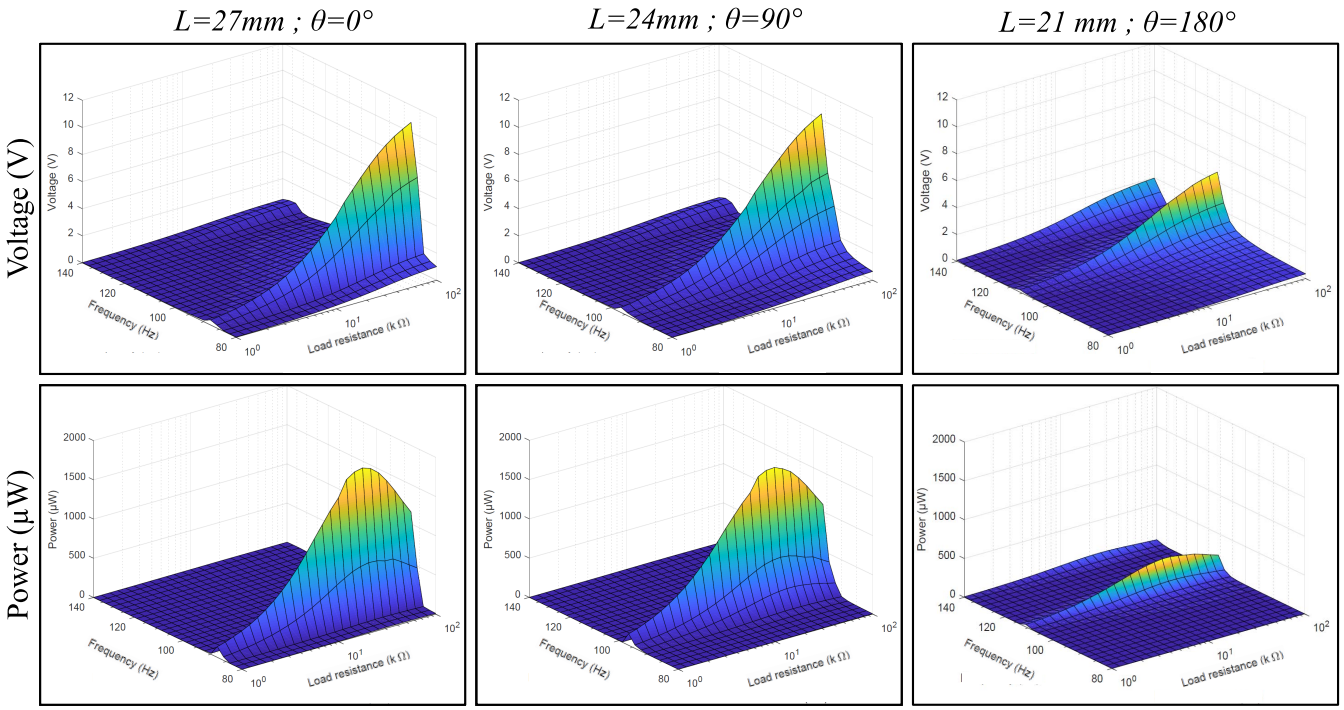

Fig. 14. Results of the experimental characterization, voltage and power as a function of load resistance and frequency.

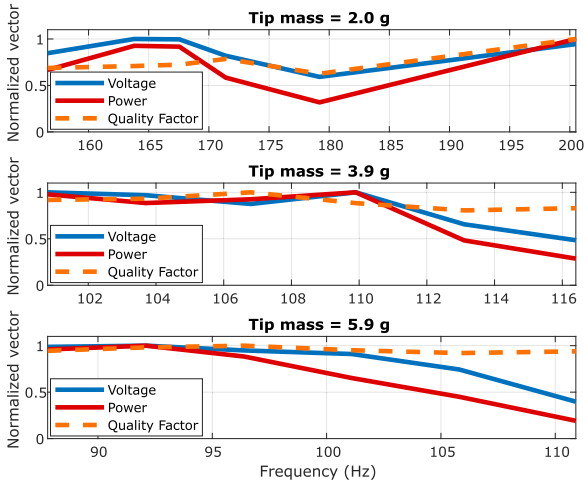

Fig. 15. Normalized optimal voltage, maximum power and quality factor evolution as a function of the resonance frequency for each mass configuration.

sufficient to power the sensor in the sleep phase and to pass the power peaks (Pmax $>$ 81.0 μW). This shows that for low acceleration amplitudes, the generator can provide enough power to maintain the sensor on at very low measurement rates, despite the extraction circuit being not adapted for this system. In the third case (Table VI), the voltage and power conditions are mostly obtained with an average voltage of 6.5 V and a power ranging from 380.0 μW to 2.0 mW.

Fig. 15 shows the evolution of the voltage, the power at the operating peak, and the quality factor normalized to the maximum value as a function of the resonance frequency (length variation) for the three tip masses. In general, the quality factor remains stable, the optimum voltage and power, decrease when resonance frequency is increasing. This reduction can be attributed to the reduction of the electromechanical coupling (Equation (6)).

$$k^2_{coupling} = \frac{\alpha^2}{kC_0} \tag{6}$$

The fact that part of the piezoelectric material, whose volume remains constant, is not subjected to mechanical stresses reduces the electromechanical conversion coefficient (α) and increases the stiffness (k). As the electrical capacity of the active element is constant, the electromechanical coupling ($k^2_{coupling}$) is reduced, and the latter decreases with increasing resonance frequency. In addition, despite the rigor implemented in the assembly, small defects ended up generating instabilities in the first vibration mode for the first case of loading (2 g) due to the small weight of the mass.

Besides low voltage levels, having an unloaded or lightly loaded beam is not recommended for this application. Without the mass, the beam itself with a minimum frequency of 260.0 Hz and a maximum of 404.0 Hz (144.0 Hz variation) limits the resonant frequency range. In ascending order of loadings, the frequency range is 44.0 Hz, 23.1 Hz, and 22.3 Hz. This shows the influence of the load on the attainable frequency range. In the case of the 5.9 g load, the range is seven times greater than the natural average bandwidth of the configuration, allowing a sensor to be powered over a wider frequency range.

C. Validation Test With WSN

1) WSN Consumption: JENNIC JN5148: The WSN to be powered is a JENNIC JN5148 module in the "End Device" configuration (Fig. 16) capable of measuring and transmitting two temperatures signals and its supply voltage. A second WSN module in the "Coordinator" configuration ensures the radio connection. Since the supply voltage of these modules

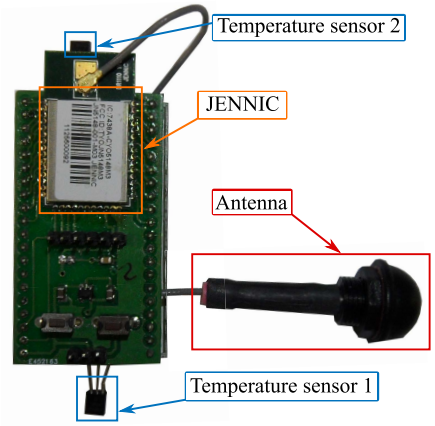

Fig. 16. JENNIC JN5148 "End Device" module.

TABLE VII
OPERATION PHASES CHARACTERISTICS

Phase	Energy (mJ))	Duration (s)	Peak power (mW)
Initialization	389.4	311.0	180.8
Meas. & trans.	3.2	0.1	213.2
Sleep	3.8	46.9	87.5

ranges from 2.8 V to 3.6 V, they were powered with 3.3 V for tests.

This WSN has three main operating phases: the initialization phase (which includes the coldstart), the connection to the network, and a 307 s transitive period of the module (a message is sent every 5 s to help verifying the quality of the signal reception). Then WSN switches between the measurement & transmission phase and the sleep mode phase. The energy, duration, and maximum peak power of these phases are listed in Table VII.

2) Laboratory Test: Installation Process Validation: To validate the operation of the overall structure (adjustment of the beam resonant frequency, energy management electronics and sensor power supply), a 40 h duration test was carried out. An arbitrary source (128.8 Hz @ 14 m/s^2) on the test bench (Fig. 12) has been chosen. This setting presents similarities with the source measured on the burner. The piezoelectric beam has been configured to resonate close to the source frequency. The prototype is fine adjusted at the source with the MPPF module (Fig. 8), whose use procedure is detailed in section III.C. The piezoelectric element is able to deliver a maximum power of 3.7 mW. After starting WSN, the storage voltage remains at about 6.7 V despite some fluctuations of the source acceleration. The operating procedure of the electronic circuit is follows to the previous description.

3) Experimental Test on Industrial Source: Vacuum Pump: A 22 h duration test of the prototype on a vacuum pump (Fig. 3) was carried out. During this test, the excitation was of 2.7 m/s^2 acceleration at a frequency of 49.0 Hz. Fig. 17 shows the storage voltage (V_{sc}), the supply voltage (V_{out}), and the current drawn by WSN. The storage is initially empty. The prototype is adjusted at the source using the MPPF module (Fig. 8) targeting the maximum voltage of the piezoelectric

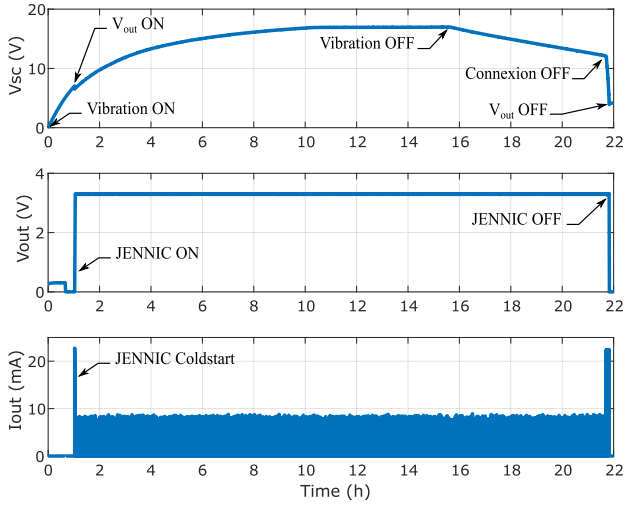

Fig. 17. 22 h duration test of final device with WSN.

beam of the order of 18.5 V. A "full" charging sequence was performed, followed by a cut-off of the excitation source and finally a cut-off of the connection between WSNs.

With a power of 2.9 mW, the activation voltage of 7.0 V is reached after 1 hour of charging and enables the "end device" WSN to be started. The storage voltage reaches a maximum of 17.0 V after 10 h of charging. After 15 h and 40 min, the generator is removed from the vibration source and the sensor continues to operate. After 21 h and 42 min, the connection to the coordinator is disconnected, and the voltage level is 12.0 V. The output switches off at a voltage level of 3.9 V after 35 connection attempts for about 10 min. The low threshold is normally 3.7 V when the current consumption is low. In this case, the inrush current required to start WSN creates a slight voltage drop, deactivating the output at a higher level. The residual voltage level of the supercapacitors allows for a second, faster start-up. According to the discharge slope of the storage space when the source is switched off, an autonomy of 6 h and 24 min is estimated. During this period the sensor continues to operate normally with repeated measurement, transmission and sleep mode cycles. This test shows that the prototype can provide enough power in case of source problems or connectivity problems between WSNs.

The efficiency between storage and consumption is calculated during the phase when the excitation is switched off. The stored energy at the beginning of the phase is 17.2 J and at the end of the phase is 8.2 J, which gives a difference of 9.0 J. The energy consumed by WSN during this phase is 3.2 J (calculated from measurements of current and supply voltage). The actual overall efficiency is then 36%. The low efficiency is partially due to the supercapacitors losses (significant self-discharge and balancing) over the long term and the poor efficiency of buck at low output current.

V. CONCLUSION

A one of a king adjustable vibration energy harvester for the industrial environment is proposed. An experimental approach details the characterization benches and the design strategy implemented for building the demonstrator. It is always necessary to know WSN consumption to dimension the energy

storage space and its source to determine the best configuration of the VEH. The device, which is made of commercially available components, showed capability of perpetually supplying energy to a low power WSN, even in the event of source variations. A mechanical system for adjusting the resonance frequency of the VEH during installation permits it to be easily tuned on site with the vibration source to maximize the recovered power. A low cost device for measurements of vibration energy potentials on industrial sites was also presented. These data show the possibility and the interest of using piezoelectric harvesters.

The VEH generator consists of a MIDE PPA 1014 piezoelectric beam in cantilever mounting. The resonance frequency of this structure is tuned coarsely by the size of seismic mass and finely by adjusting the length of the beam. A system integrated into the encapsulation enables the adjustment to be carried out by turning a cam. A dedicated measuring device has been developed to visualize the output voltage of the piezoelectric element in order to find the optimal adjustment. When the generator is subjected to external vibrations (from an industrial electric motor for example), the piezoelectric beam produces electrical charges. These charges are harvested using an LTC3588-1 extraction circuit that stores them in a dedicated space before shaping the electrical energy to power the sensor. The storage space is composed of eight 1 F supercapacitors in series. The stored energy can go up to 24.2 J. A storage is necessary to compensate the fluctuations and the consumption peaks from WSN. A delayed power activation system authorizes storage of the energy necessary to ensure several start-up phases.

The final demonstrators presented are configured to operate in frequency ranges from 48.0 Hz to 66.0 Hz and from 69.0 Hz to 94.4 Hz. These demonstrators are compatible with the vibration sources presented in the article and they are able to run perpetually a WSN (as long as vibrations exist). In comparison with the literature's harvesters, we propose a demonstrator with an average variation of 27 % compared to the maximum resonance frequency and a power of 2.9 mW when accelerated at 2.7 m/s^2. Although the operating range is narrower than others generators, the power is higher. Compared to non-linear solutions and able to supply sensors, the power levels are lower over comparable operating ranges. However, the implementation is simpler and more robust.

The proposed solution shows robustness to the hazards of vibration sources. It can overcome the fluctuation of acceleration during storage. It can also accept small frequency variations (low bandwidth). In the case of significantly high variations of the latter, it is necessary to adjust the resonance frequency of the VEH. Fortunately, for many applications the frequency do not change over the time.

Acknowledgment

The authors would like to thank Xavier Dollat and Ricardo Knoblauch for their invaluable support in this work.

References

[1] Libelium. *Libelium Smart World*. Accessed: Jun. 8, 2021. [Online]. Available: https://www.libelium.com

[2] S. Kim *et al.*, "Health monitoring of civil infrastructures using wireless sensor networks," presented at the 6th Int. Symp. Inf. Process. Sensor Netw., Apr. 2007, doi: 10.1109/IPSN.2007.4379685.

[3] A. Mainwaring, D. Culler, J. Polastre, R. Szewczyk, and J. Anderson, "Wireless sensor networks for habitat monitoring," presented at the 1st ACM Int. Workshop Wireless sensor Netw. Appl., 2002, doi: 10.1145/570738.570751.

[4] G. Werner-Allen *et al.*, "Deploying a wireless sensor network on an active volcano," *IEEE Internet Comput.*, vol. 10, no. 2, pp. 18–25, Mar. 2006, doi: 10.1109/MIC.2006.26.

[5] J. Gubbi, R. Buyya, S. Marusic, and M. Palaniswami, "Internet of Things (IoT): A vision, architectural elements, and future directions," *Future Generat. Comput. Syst.*, vol. 29, no. 7, pp. 1645–1660, 2013, doi: 10.1016/j.future.2013.01.010.

[6] Ovum. *Ovum IoT Entrep. Insight Survey*. Accessed: Jun. 8, 2021. [Online]. Available: https://omdia.tech.informa.com/

[7] S. Basagni, M. Y. Naderi, C. Petrioli, and D. Spenza, "Wireless sensor networks with energy harvesting," in *Mobile Ad Hoc Networking*. Hoboken, NJ, USA: Wiley, 2013, pp. 701–736, doi: 10.1002/9781118511305.ch20.

[8] S. Priya and D. J. Inman, Eds., *Energy Harvesting Technologies*. Cham, Switzerland: Springer, 2009, doi: 10.1007/978-0-387-76464-1.

[9] T. Starner, "Human-powered wearable computing," *IBM Syst. J.*, vol. 35, nos. 3–4, pp. 618–629, 1996, doi: 10.1147/SJ.353.0618.

[10] M. Stordeur and I. Stark, "Low power thermoelectric generator-self-sufficient energy supply for micro systems," presented at the 16th Int. Conf. Thermoelectrics, 1997, doi: 10.1109/ICT.1997.667595.

[11] S. Roundy, P. K. Wright, and J. Rabaey, "A study of low level vibrations as a power source for wireless sensor nodes," *Comput. Commun.*, vol. 26, no. 11, pp. 1131–1144, Jul. 2003, doi: 10.1016/s0140-3664(02)00248-7.

[12] S. Roundy, "On the effectiveness of vibration-based energy harvesting," *J. Intell. Mater. Syst. Struct.*, vol. 16, pp. 809–823, Oct. 2005, doi: 10.1177/1045389x05054042.

[13] S. Beeby and W. Neil, *Energy Harvesting for Autonomous Systems*. Norwood, MA, USA: Artech House, 2010.

[14] M. Lallart, *Small-Scale Energy Harvesting*. London, U.K.: IntechOpen, 2012.

[15] Perpetuum. *Perpetuum PMG*. Accessed: Jun. 8, 2021. [Online]. Available: https://perpetuum.com/

[16] Star. *Vibration Harvester Unit*. Accessed: Jun. 8, 2021. [Online]. Available: http://www.star-m.jp/eng/service/de_catalog/vpg-eh_2_en.pdf

[17] T. Masaki *et al.*, "Multi-frequency vibration-driven electret generator for wireless sensor applications," *J. Phys., Conf.*, vol. 557, Nov. 2014, Art. no. 012074, doi: 10.1088/1742-6596/557/1/012074.

[18] MicroGen Systems. *BOLT*. Accessed: Jun. 8, 2021. [Online]. Available: https://www.analog.com/en/technical-articles/microgen-s-piezo-mems-vibration-energy-harvesters-enable-linear-technology-smartmesh-ip-wireless.html

[19] D. Su, K. Nakano, R. Zheng, and M. P. Cartmell, "On electrical optimisation using a duffing-type vibrational energy harvester," *Proc. Inst. Mech. Eng. C, J. Mech. Eng. Sci.*, vol. 229, no. 18, pp. 3308–3319, Dec. 2014, doi: 10.1177/0954406214563736.

[20] F. Huet, F. Formosa, A. Badel, J.-F. Capsal, and M. Lallart, "Vibration energy harvesting device using P(VDF-TrFE) hybrid fluid diaphragm," *Sens. Actuators A, Phys.*, vol. 247, pp. 12–23, Aug. 2016, doi: 10.1016/j.sna.2016.05.029.

[21] D. Karličić, T. Chatterjee, M. Cajić, and S. Adhikari, "Parametrically amplified mathieu-duffing nonlinear energy harvesters," *J. Sound Vib.*, vol. 488, Dec. 2020, Art. no. 115677, doi: 10.1016/j.jsv.2020.115677.

[22] Y. Jia, "Review of nonlinear vibration energy harvesting: Duffing, bistability, parametric, stochastic and others," *J. Intell. Mater. Syst. Struct.*, vol. 31, no. 7, pp. 921–944, Feb. 2020, doi: 10.1177/1045389x20905989.

[23] S. C. Stanton, C. C. McGehee, and B. P. Mann, "Nonlinear dynamics for broadband energy harvesting: Investigation of a bistable piezoelectric inertial generator," *Phys. D, Nonlinear Phenomena*, vol. 239, no. 10, pp. 640–653, May 2010, doi: 10.1016/j.physd.2010.01.019.

[24] W. Q. Liu, A. Badel, F. Formosa, Y. P. Wu, and A. Agbossou, "Novel piezoelectric bistable oscillator architecture for wideband vibration energy harvesting," *Smart Mater. Struct.*, vol. 22, no. 3, Feb. 2013, Art. no. 035013, doi: 10.1088/0964-1726/22/3/035013.

[25] L. Dong, M. G. Prasad, and F. T. Fisher, "Two-dimensional resonance frequency tuning approach for vibration-based energy harvesting," *Smart Mater. Struct.*, vol. 25, no. 6, Jun. 2016, Art. no. 065019.

[26] V. R. Challa, M. G. Prasad, Y. Shi, and F. T. Fisher, "A vibration energy harvesting device with bidirectional resonance frequency tunability," *Smart Mater. Struct.*, vol. 17, no. 1, Feb. 2008, Art. no. 015035.

[27] P. Podder, P. Constantinou, D. Mallick, A. Amann, and S. Roy, "Magnetic tuning of nonlinear MEMS electromagnetic vibration energy harvester," *J. Microelectromech. Syst.*, vol. 26, no. 3, pp. 539–549, Jun. 2017, doi: 10.1109/JMEMS.2017.2672638.

[28] R. Dauksevicius *et al.*, "Nonlinear piezoelectric vibration energy harvester with frequency-tuned impacting resonators for improving broadband performance at low frequencies," *Smart Mater. Struct.*, vol. 28, no. 2, Jan. 2019, Art. no. 025025, doi: 10.1088/1361-665x/aaf358.

[29] E. D. Niri and S. Salamone, "A passively tunable mechanism for a dual bimorph energy harvester with variable tip stiffness and axial load," *Smart Mater. Struct.*, vol. 21, no. 12, Nov. 2012, Art. no. 125025, doi: 10.1088/0964-1726/21/12/125025.

[30] Y. Kuang, Z. J. Chew, J. Dunville, J. Sibson, and M. Zhu, "Strongly coupled piezoelectric energy harvesters: Optimised design with over 100 mW power, high durability and robustness for self-powered condition monitoring," *Energy Convers. Manage.*, vol. 237, Jun. 2021, Art. no. 114129, doi: 10.1016/j.enconman.2021.114129.

[31] S. Priya *et al.*, "A review on piezoelectric energy harvesting: Materials, methods, and circuits," *Energy Harvesting Syst.*, vol. 4, no. 1, pp. 3–39, Aug. 2019, doi: 10.1515/ehs-2016-0028.

[32] Y. Wang, H. He, and R. Xu, "An analytical model for a piezoelectric vibration energy harvester with resonance frequency tunability," *Adv. Mech. Eng.*, vol. 7, no. 6, Jun. 2015, Art. no. 168781401559029, doi: 10.1177/1687814015590298.

[33] S.-C. Huang and K.-A. Lin, "A novel design of a map-tuning piezoelectric vibration energy harvester," *Smart Mater. Struct.*, vol. 21, no. 8, Aug. 2012, Art. no. 085014, doi: 10.1088/0964-1726/21/8/085014.

[34] J. Schaufuss, D. Scheibner, and J. Mehner, "New approach of frequency tuning for kinetic energy harvesters," *Sens. Actuators A, Phys.*, vol. 171, no. 2, pp. 352–360, Nov. 2011, doi: 10.1016/j.sna.2011.07.022.

[35] J. Chandwani, R. Somkuwar, and R. Deshmukh, "Multi-band piezoelectric vibration energy harvester for low-frequency applications," *Microsyst. Technol.*, vol. 25, no. 10, pp. 3867–3877, Jan. 2019, doi: 10.1007/s00542-019-04321-6.

[36] R. Somkuwar, J. Chandwani, and R. Deshmukh, "Wideband auto-tunable vibration energy harvester using change in centre of gravity," *Microsyst. Technol.*, vol. 24, no. 7, pp. 3033–3044, Mar. 2018, doi: 10.1007/s00542-018-3846-x.

[37] Linear Technology Corporation. *LTC3588-1*. Accessed: Jun. 8, 2021. [Online]. Available: http://www.analog.com/en/products/ltc3588-1.html

[38] L. Chen, X. Xu, P. Zeng, and J. Ma, "Integration of energy harvester for self-powered wireless sensor network nodes," *Int. J. Distrib. Sensor Netw.*, vol. 10, no. 4, Apr. 2014, Art. no. 782710, doi: 10.1155/2014/782710.

[39] X. Zhang, J. Fang, F. Meng, and X. Wei, "A novel self-powered wireless sensor node based on energy harvesting for mechanical vibration monitoring," *Math. Problems Eng.*, vol. 2014, pp. 1–5, Jan. 2014, doi: 10.1155/2014/642365.

[40] Y. G. Jiang, S. Shiono, H. Hamada, T. Fujita, K. Higuchi, and K. Maenaka, "Lowfrequency energy harvesting using a laminated PVDF cantilever with a magnetic mass," in *Proc. PowerMEMS*, Leuven, Belgium, 2010, pp. 375–378.

[41] A.-M. Stamatellou and A. I. Kalfas, "Experimental investigation of energy harvesting from swirling flows using a piezoelectric film transducer," *Energy Convers. Manage.*, vol. 171, pp. 1405–1415, Sep. 2018, doi: 10.1016/j.enconman.2018.06.081.

[42] A. Morel, G. Pillonnet, P. Gasnier, E. Lefeuvre, and A. Badel, "Frequency tuning of piezoelectric energy harvesters thanks to a short-circuit synchronous electric charge extraction," *Smart Mater. Struct.*, vol. 28, no. 2, Dec. 2018, Art. no. 025009, doi: 10.1088/1361-665x/aaf0ea.

[43] A. Brenes *et al.*, "Large-bandwidth piezoelectric energy harvesting with frequency-tuning synchronized electric charge extraction," *Sens. Actuators A, Phys.*, vol. 302, Feb. 2020, Art. no. 111759, doi: 10.1016/j.sna.2019.111759.

[44] A. Morel *et al.*, "Fast-convergence self-adjusting SECE circuit with tunable short-circuit duration exhibiting 368% bandwidth improvement," *IEEE Solid-State Circuits Lett.*, vol. 3, pp. 222–225, 2020, doi: 10.1109/LSSC.2020.3012340.

[45] Linear Technology Corporation. *LTC1540*. Accessed: Jun. 8, 2021. [Online]. Available: https://www.analog.com/en/products/ltc1540.html

[46] F. Huet, U. d. Toulouse. F. LAAS-CNRS, and V. Boitier, "Design strategy of conventional electronic for wireless sensor node powered by vibration energy harvester," *Renew. Energy Power Quality J.*, vol. 17, pp. 555–560, Jul. 2019, doi: 10.24084/repqj17.375.

[47] MIDE. *PPA PRODUCTS Datasheet & User Manual*. Accessed: Jun. 8, 2021. [Online]. Available: https://www.mide.com/mide-resources

Florian Huet received the master's degree in mechanics and the Ph.D. degree in engineering sciences from the University of Grenoble Alps in 2011 and 2016, respectively. Since 2019, he has been an Associate Professor with the LISPEN Laboratory, ENSAM. His research activities are oriented in the field of ambient energy harvesting (vibration, wind, solar, and thermal) for electrical conversion and used by macro and microelectronic systems.

Vincent Boitier received the Teacher Training degree in applied physics in 1992 and the Ph.D. degree in automatic industrial computing from the National Institute of Applied Science (INSA), Toulouse, in 1996. He is currently a Former Student with the Ecole Normale Supérieure de Cachan, France. Since 1997, he has been an Associate Professor with the University Paul Sabatier Toulouse III and the LAAS-CNRS Laboratory. His research interests include medium and low power photovoltaic applications, small-power energy harvesting for wireless systems, and analysis of the energy potential of intermittent renewable sources (photovoltaic, wind, and thermal).

Lionel Seguier received the degree in electrical engineering in 2006. He is currently a Former Student with the Conservatoire National des Arts et Métiers (CNAM), France. Since 2006, he has been an Engineer at the LAAS CNRS Laboratory, and works on the development of systems, such as DC/DC converter, renewable energies, electrochemical storage, and energy harvesting for IoT.